Holo-interferometric Studies of Thermal Deformations in Microelectronic Modules

T. D. Dudderar
AT&T Bell Laboratories
600 Mountain Avenue
Murray Hill, New Jersey 07974

P. M. Hall
AT&T Bell Laboratories
555 Union Boulevard
Allentown, Pennsylvania 18103

J. A. Gilbert
Associate Professsor of Engineering Mechanics
University of Wisconsin-Milwaukee
Milwaukee, Wisconsin 53201

ABSTRACT

Evaluations of the thermally induced warping in various microcircuit modules have been made using holographic interferometry. It was found that in many cases the measured out-of-plane displacement pattern of the multilayer printed wiring board was highly complex, of changing shape and/or stable only after several test cycles. Furthermore, qualitative analysis of these results demonstrate that mechanical structure can have a significant influence on the loadings experienced by the solder post connections between a surface mounted ceramic chip carrier and its printed wiring board during normal power cycles.

1. Introduction

Leadless ceramic chip carriers of the type used in advance design microcircuit modules have numerous advantages over leaded device mounting systems.[1-3] These include lower cost, greater ruggedness against handling damage, and simpler, more compact structures with fewer joints. However, the solder posts connecting a leadless ceramic chip carrier to its multilayer printed wiring board experience significant strains during normally occurring temperature changes, and these can lead to cracks and early failure.[4,5] Such strains arise primarily because of differences in the thermal-mechanical responses of the leadless ceramic chip carrier and the printed wiring board, and can be attributed to: (a) the large difference in the thermal expansion characteristics of these components (most notably during thermal chamber or oven cycling[6]) and (b) the development of large temperature gradients (most notably during power cycling[7]), and (c) the presence of structural asymmetries on the printed wiring board stackup. The incorporation of two symmetrically disposed copper clad invar (CCI) layers, each of around 140 μm total thickness, into the sublayer structure of the multilayer printed wiring board provides a direct mechanical means of significantly reducing the in-plane thermal expansion mismatch part of the problem.

Under the conditions of (1) highly localized temperature gradients that occur during power dissipation, (2) complex thermo-mechanical interactions between the surface mounted leadless ceramic chip carriers and the printed wiring board, and (3) the variations in local stiffness associated with differences in the printed wiring board, the development of a rational understanding of the thermal response of a given module design can be achieved only through a comprehensive full field experimental evaluation. The present studies were conducted to exploit the capacity of HI for making such evaluations. The analysis of the resulting data is focussed on determining the rotations and out-of-plane deformations imposed on the interconnecting solder posts by the thermally induced warping of the complex ceramic chip carrier/printed wiring board structure.

2. State-of-the-Art Fiber Optic Holo-Interferometry

Figure 1 shows a state-of-the-art holographic interferometer in which the complicated array of beam splitters, steering mirrors, prisms and spatial filters found in traditional holographic systems have been replaced by a single low power lens or objective (for coupling), a single mode optical fiber or SMF for object illumination and, as suggested by Jones et. al.[8] a directional coupler feeding a second SMF as a variable beam splitter/reference beam. The two SMFs can be suitably dissimiliar in length as to provide the necessary optical path length matching. No spatial filtering is required as the SMFs themselves accomplish that function, as well as relaxing many of the stability requirements.[9,10] So long as the launch optics are firmly coupled into the laser, only the fiber outputs, the test specimen and the hologram itself need be rigidly mounted and isolated. Furthermore, the free space (air) propagation path lengths are significantly reduced, so that the deleterious effects of thermal air currents and moving dust are almost completely eliminated. The hologram may be recorded on any of a wide variety of media, ranging from high resolution photographic plates (emulsion on glass) which require wet processing but provide a permanent record, to sophisticated eraseable media that can be dry processed rapidly (in 1 minute or less) and in place, like a thermoplastic "instant" holocamera system. In any case the resulting holographic interference fringe field may be related to the surface deformations at each point by the simple vector expression

$$n\lambda = \hat{k} \cdot \hat{d} \qquad (1)$$

where n is the interference fringe number, λ is the wavelength of the coherent light used to record and reconstruct the hologram, $\hat{k}$ is the sensitivity vector $(\hat{i}_2 - \hat{i}_1)$ where $\hat{i}_1$ and $\hat{i}_2$ are unit vectors in the illumination and observation directions, and $\hat{d}$ is the mechanical displacement vector at the point of observation on the surface. In the tests to be described here, the flat surfaces of the (in this case) predominantly planar microelectronic modules and their surface mounted components were intentionally oriented normal to the bisector of the angle, 2β, between $\hat{i}_1$ and $\hat{i}_2$. Consequently, the holo-interferometer senses only the out-of-plane component of displacement, D. Since $\hat{k}$, the sensitivity vector, also points along the bisector, equation (1) becomes simply

$$n\lambda = 2D\cos\beta \qquad (2)$$

and the resulting fringe pattern becomes a contour mapping of the changes in surface "elevation" with a fringe to fringe separation on the order of half a wavelength, or only 0.316 μm. Obviously, different directions of observation and illumination can be chosen such that the sensitivity vector lies in a direction suitable to resolve other components of surface displacement and/or operate at another (somewhat lower) sensitivity as desired.

Applications to the Measurement of Thermal Deformations in Microelectronic Modules

Figure 2 shows reconstructions of three holo-interferograms of a CCI (Copper-Clad-Invar) type microelectronic module subjected to three successive cycles from zero to full power. This module consisted of a

single leadless ceramic chip carrier (LCCC) surface mounted (off-center) on the reverse side (as seen in the figure) of a 95 mm×55 mm printed wiring board (PWB). In each test a reference hologram was recorded with the module at room temperature and unpowered. Then power (750 mw) was applied to an element in the LCCC and, after a 20 minute interval to allow the system to reach thermal equilibrium, a second exposure was recorded on the same hologram film. The hologram was then removed for processing while the power to the sample was turned off and it was allowed to return to room temperature before the next test cycle. After processing, each of the resulting double exposed holograms (but not the sample) was reilluminated (in turn) by the original reference beam to reconstruct the holo-interferogram images photographed for Figure 2. Several things are immediately apparent from these results. First, for this type of module, the PWB warping pattern is fairly complicated, especially in regions away from the LCCC. Second, the shape and magnitude of this warping changes form cycle to cycle - Figure 2a (from the first cycle to power) shows fewer fringes and a significantly different pattern when compared to either Figure 2b or 2c for the second and third cycles. Figures 3a and 3b show computer generated isometric plots of the displacement information taken from the first and third holo-interferograms, Figures 2a and 2c. These plots clearly illustrate the differences and demonstrate that the response is not isomorphic. A succession of such test cycles can be used to determine when and if such a module stabilizes.

Of course, it is often important to evaluate the differences between modules of differing design and construction. Figures 4a and 4b show reconstructions of two double exposed interferograms and Figure 5 shows the resulting isometric out-of-plane displacement plots for two structurally different samples subjected to full power for 20 minutes. Clearly, the sample with one surface mounted LCCC warps quite differently from the one with a symmetric array of five LCCCs. Similar studies have been made to evaluate the presence or absence of internal CCI layers, the effects of an asymmetric PWB laminate stackup, changes in CCI through-hole diameter, and so forth.

While a great deal of useful information can be obtained using the double exposure technique, real-time holo-interferometry provides an even more powerful approach to evaluating time varying phenomena. Figure 6 shows a series of twelve real-time holo-interferograms recorded by photographing the developing fringe field as seen on the same sample shown in the double-exposed hologram of Figure 2. These evolving interference fringe patterns were recorded, along with thermocouple readings taken from within the LCCC itself, over a forty minute period following the application of full power. Figure 7, which shows plots of both the LCCC temperature and the maximum fringe order (or displacement of the PWB) against time, clearly demonstrates that for this particular sample thermally induced PWB deformation continues to increase long after the LCCC thermocouple has reached thermal equilibrium.

While all such "global" evaluations of the deformation response are interesting, a better understanding of what actually takes place requires a more detailed consideration of how such structures behave.

3. Solder Post Deformation

The solder connection between a leadless surface mounted component (like a LCCC) and its mounting surface (like a PWB) must accommodate the deformation imposed by the thermal expansion mismatch, temperature gradient and so forth that arise during heating. This accommodation may be described in terms of the three modes of deformation shown in Figure 8*. These modes are described as Mode A, associated associated with the in-plane displacement (or shear), Mode B associated with the out-of-plane rotation (or bending), and Mode C, associated with the out-of-plane displacement (tension or compression). Mode A deformation can be estimated from in-plane strain gage measurements, while Modes B and C can be most readily evaluated from out-of-plane holo-interferometric data of the type shown in Figures 2 through 6.

Geometry requires that, in a square or rectangular array of solder posts, the corner posts will experience the greater Mode A deformation, being farthest apart. Out-of-plane bending of the PWB below the LCCC causes the straight row of posts along any side of the LCCC to experience varying distributions of Modes B and C deformation as well. For example, in power cycling thermal gradients generally dominate and cause the PWB to form a "hill" below the LCCC as shown in Figure 3. In this case the Mode C deformation varies from tension at the corner to compression along the sides at mid-span, Figure 8. Furthermore, in power cycling Mode B goes negative as the PWB bends *towards* the LCCC at its center. In chamber cycling the thermal expansion mismatch dominates the deformation, there being little or no thermal gradient, and the PWB reponds by moving *away* from the LCCC during heating. In this event, while Mode A remains positive, Modes B and C deformation both change sign. Obviously, in an actual in-service environment the module would experience both (1) an overall warming due to heat generated by surrounding modules and (2) severe thermal gradients due to power dissipation from the LCCC itself. Consequently, the deformation response will depend on the interplay between these two factors and the temperature dependent mechanical properties of the PWB and the solder posts themselves. Consequently, an in-situ real-time holo-interferometric evaluation is usually the most reliable way to determine the actual form of the response.

Whatever the thermal loading conditions to be considered, sensitive out-of-plane holo-interferometric measurements can provide a great deal of quantitative information about both (1) the changing displacement gradients which completely define the Mode B bending at each joint, and (2) the relative out-of-plane extensions or compressions which define the Mode C deformation. Figure 9 shows a profile of the out-of-plane deformation distribution plotted around the four sides of the LCCC derived from the data taken at full power on the first sample shown in Figures 2c and 3b. In the analysis of this data a "tilt" plane representing the orientation of an inflexible LCCC (relative to the PWB) was calculated by positioning the "best fit" plane to give a zero net for the sum of all the solder post extensions. The deviations of the out-of-plane deformation profile from this "tilt" plane represents the extensions (or compressions) of the solder posts, and are shown as heavy vertical lines at each solder post location around the LCCC. These results may be converted to Mode C deformations of appropriate sign by dividing by the solder post stand-off height.

4. Conclusions

Fiber optic holo-interferometry provides a practical means of evaluating full field surface deformations (in real-time if desired) on objects such as microelectronic modules, whose complexity would render almost any other technique, experimental or analytical, difficult or impossible. Such tests require a minimum of sample preparation and little more time than that required by the dynamics of the sample to reach the desired response. The wavelength sensitivity of this technique is sufficient to detect subtle differences in the internal construction of complex but physically small structures under a variety of either prototype or less than prototype loadings. In the present examples, thermally induced PWB deformations due to power dissipation from surface mounted components can be readily analyzed in detail to determine the deformations experienced by individual solder connections. This same approach may be applied to the detailed evaluation of the deformation response of any complex structure associated with microelectronic technology and subjected to any of a variety of loadings, including mechanical forces and even vibration. Finally, the addition of a vidicon camera/digitizer system to record the resulting holo-interferometric fringe fields as they develop, when coupled with a fast laboratory computer/image processor with appropriately designed softwave, eventually provides a very powerful production tool for component evaluation on a very nearly real-time basis.

---

* This figure is drawn assuming the component remains essentially flat while the PWB deforms. While this may not be true in general, it is illustrative and does apply reasonably well under certain conditions (a component that is stiffer than the PWB, or thermally softened solder, etc).

5. Acknowledgements

The authors wish to acknowledge the efforts of many corraborators working in various fields. These include, most significantly, P. J. Lemaire of AT&T Bell Laboratories, Murray Hill, who provided single mode fiber optic illuminators, M. Rao of AT&T Bell Laboratories, Richmond, who sent us so many interesting sample modules for evaluation, and Don Bloechle for the structural analysis which determined the PWB stack up. Since 1980 Prof. Gilbert's efforts with fiber optics have been supported in part by contracts DAAG-29-80-K-0028 and DAAG-29-84-K-0183 with the U.S. Army Research Office in Research Triangle Park, NC.

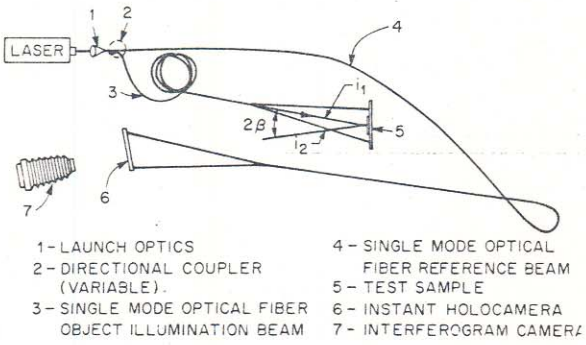

Figure 1 - Schematic of a Fiber Optic Holographic System for Local Double Exposure or Real-Time Holo-Interferometry.

REFERENCES

(1) D. I. Amey, "Integrated Circuit Package Selection: Pin Grid Array vs. Chip Carriers," Electronic Packaging and Production, January, 1982, p. 262-278.

(2) J. E. Byrum and W. Bischoff, "Manufacturing Low Cost Chip Carriers," Proc. Internation Microelectronics Symposium, Oct., 1981, p. 309-314.

(3) J. E. Fennimore, "Hermetic Ceramic Chip Carrier Implementation," Electronic Packaging and Production, May, 1981, p. 172-181.

(4) C. L. Lassen, "Use of Metal Core Substrates for Leadless Chip Carrier Interconnection". Electronic Packaging and Production, March, 1981, p. 98-104.

(5) C. A. Harper and W. W. Staley, "Some Critical Materials Factors in the Application of Leadless Chip Carrier Packages," Electronic Packaging and Production, August, 1981, p. 134-142.

(6) P. M. Hall "Strain Measurements During Thermal Chamber Cycling of Leadless Ceramic Chip Carriers Soldered to Multilayer Printed Wiring Boards," Proceedings of the 1984 Electronic Materials Conference.

(7) P. M. Hall, T. D. Dudderar and J. F. Argyle, "Thermal Deformation Observed in Leadless Ceramic Chip Carriers Surface Mounted to Printed Wiring Boards". IEEE Trans., Components, Hybrids and Manufacturing Technology Vol. CHMT-6 Dec., 1983, p. 544-552.

(8) J. D. C. Jones, M. Corke, A. D. Kersey and D. A. Jackson, "Single-mode Fibre-optic Holography," J. Phys. E: Sci. Instrum., 17, 1984, p. 271-273.

(9) J. A. Gilbert, T. D. Dudderar, M. E. Schultz and A. J. Boehnlein, "The Monomode Fiber - A New Tool for Holographic Interferometry," Experimental Mechanics, *23* (3) June, 1983, p. 190-195.

(10) J. A. Gilbert, T. D. Dudderar and A. Nose, "Remote Deformation Field Measurement Through Different Media Using Fiber Optics," Proc. 1983 Spring Conf. of the SESA, May 15-19, 1983, p. 424-430.

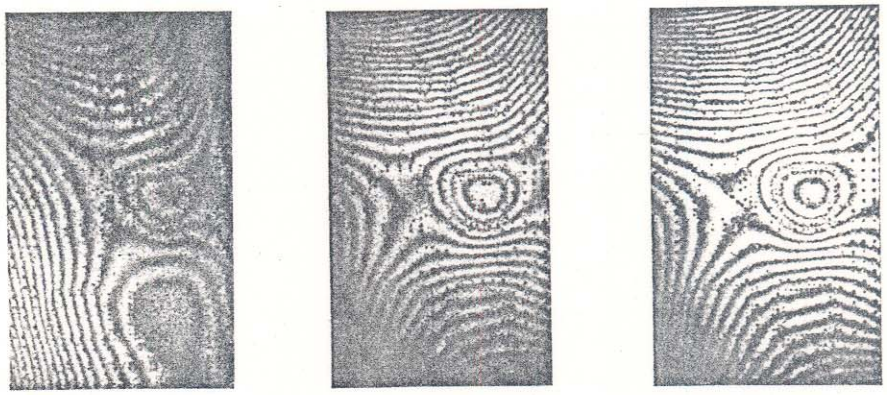

Figure 2 - Reconstructions of Double Exposed Holo-Interferograms of an LCCC Sample Module (After 20 minutes) Powered to 0.75 Watts on Three Successive Cycles.

Figure 3 - Computer Generated Isometric Data Plots of the Holo-Interferometrically Measured Out-of-Plane Displacement Distributions on the First and Third Thermal Loading Cycles.

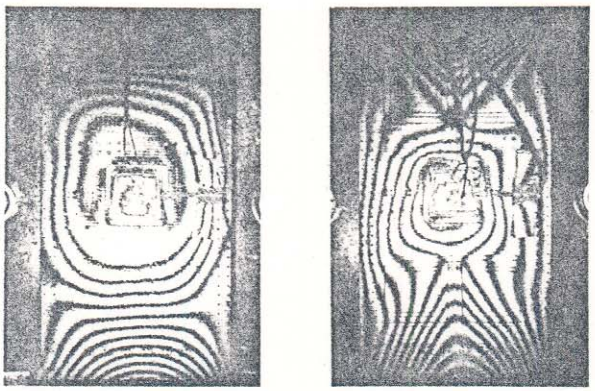

Figure 4 - Reconstructions of Double Exposed Holo-Interferograms of Two Different Sample Modules with (a) Five and (b) One LCCC.

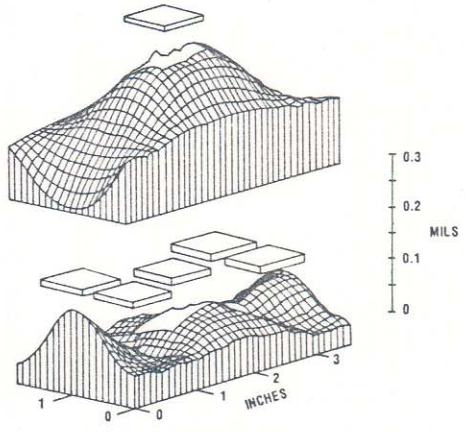

Figure 5 - Computer Generated Isometric Data Plots of the Holo-Interferometrically Measured Out-of-Plane Displacement Distributions for Samples with One and Five LCCCs respectively.

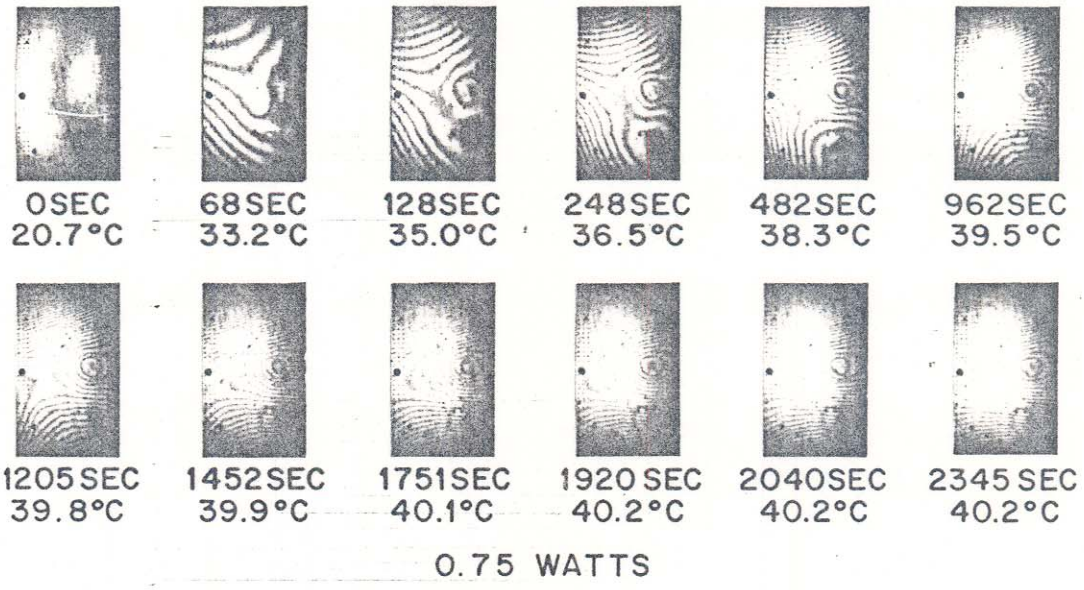

Figure 6 - Real-Time Holo-Interferograms Recorded After the Application of 0.75 Watts to the First Sample Module.

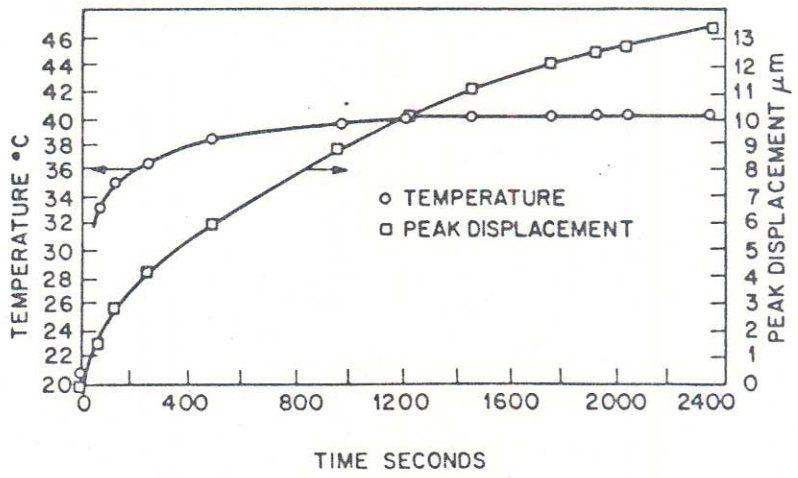

Figure 7 - Temperature versus Time and Maximum Out-of-Plane Displacement Data versus Time for the First Sample Module at 0.75 Watts of Power Dissipation.

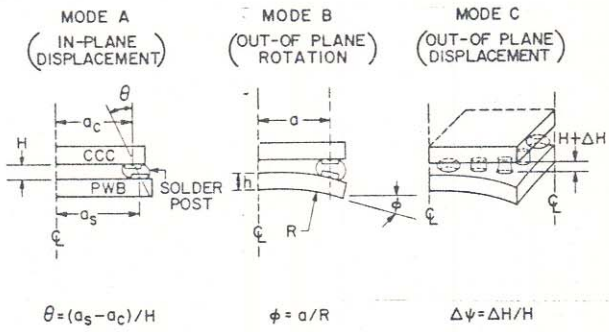

Figure 8 - Solder Post Deformation Modes for Power Heating.

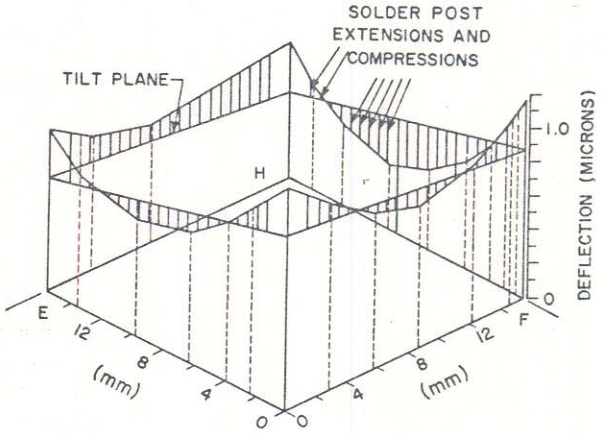

Figure 9 - Isometric Plot of the Out-of-Plane Thermal Deformations of the First Sample Module Evaluated at the Solder Posts Connecting the LCCC to the PWB (After 20 Minutes at 0.75 Watts).